International Journal of Extreme Manufacturing

Burst mode enabled ultrafast laser inscription inside gallium arsenide

OPEN ACCESS
IOP Publishing | IMMT
International Journal of Extreme Manufacturing
Int. J. Extrem. Manuf. 4 (2022) 045001 (9pp)
https://doi.org/10.1088/2631-7990/ac8fc3

Burst mode enabled ultrafast laser inscription inside gallium arsenide

Andong Wang*, Pol Sopeña and David Grojo*

Aix-Marseille University, CNRS, LP3, UMR7341, 13009 Marseille, France

E-mail: Andong.wang@univ-amu.fr and David.grojo@univ-amu.fr

Received 21 February 2022, revised 1 April 2022
Accepted for publication 6 September 2022
Published 21 September 2022

Abstract

Ultrafast laser inscription (ULI) inside semiconductors offers new perspectives for 3D monolithic structures to be fabricated and new functionalities to be added in electronic and photonic microdevices. However, important challenges remain because of nonlinear effects such as strong plasma generation that distort the energy delivery at the focal point when exposing these materials to intense infrared light. Up to now, the successful technological demonstrations have primarily concentrated on silicon (Si). In this paper, we target at another important semiconductor: gallium arsenide (GaAs). With nonlinearities higher than those of Si, 3D-machining of GaAs with femtosecond pulses becomes even harder. However, we show that the difficulty can be circumvented by burst-mode irradiation. We generate and apply trains of pulses at terahertz repetition rates for efficient pulse-to-pulse accumulation of laser-induced free carriers in the focal region, while avoiding an overdose of prefocal excitations. The superior performance of burst-mode irradiation is confirmed by a comparative study conducted with infrared luminescence microscopy. The results indicate a successful reduction of the plasma density in the prefocal region so that higher pulse energy reaches the focal spot. The same method is applied to identify optimum irradiation conditions considering particular cases such as asymmetric pulse trains and aberrated beams. With 64-pulse trains, we successfully manage to cross the writing threshold providing a solution for ULI inside GaAs. The application potential is finally illustrated with a stealth dicing demonstration by taking benefit of the burst mode. The irradiation method opens wide possibilities for 3D structuring inside GaAs by ULI.

Supplementary material for this article is available online

Keywords: laser processing, ultrafast laser inscription, THz-repetition-rate, burst, semiconductors, gallium arsenide

1. Introduction

Ultrafast laser inscription (ULI) offers unique possibilities to directly integrate precise and functional micro/nano structures inside transparent solids. This creates 3D architectured microsystems that are not easily achievable by other manufacturing technologies such as lithography [1]. Past decades have witnessed a broad range of possible applications of ULI from the fabrication of photonic microdevices [2, 3] to bio-compatible systems [4]. However, most of these applications remain limited to large bandgap materials transparent to visible light. Recent advances have revealed the feasibility of ULI inside semiconductor materials with infrared intense lasers [5–8], but a much more challenging situation is faced due to the very different properties given the narrow bandgap. In particular, the higher refractive indices and much stronger propagation nonlinearities tend to delocalize the energy flux and deteriorate the laser focusing conditions, preventing in most cases to achieve enough energy density for ULI deep

* Authors to whom any correspondence should be addressed.

2631-7990/22/045001+9$33.00

inside semiconductors. In this regard, a practical and reliable solution to this problem remains highly desirable. This would broaden the range of applications of ULI and provide a novel manufacturing technology for important sectors as microelectronics and the growing field of semiconductor photonics.

Recent efforts in this direction have concentrated on silicon (Si), the basis material in the electronics industry. Experimental approaches that deviate from standard laser machining configurations have been implemented to circumvent the limitations of energy delivery inside Si [7, 9–11]. However, so far there have been very few works [12] investigating other semiconductors like gallium arsenide (GaAs) which is important for various technologies such as light-emitting diodes, nonlinear crystals, and photovoltaic cells. In this context, it is interesting to point important differences between GaAs and Si. For example, GaAs exhibits a direct bandgap and a two-photon absorption coefficient of 7 cm GW^{-1} at 300 K and 1.55 μm [13] whereas Si has a indirect bandgap with a two-photon absorption coefficient of just 0.76 cm GW^{-1} for similar conditions [14]. In addition, GaAs has a nonlinear refractive index which is more than five times higher than that of Si. From these properties, one can predict the appearance of even stronger plasma and nonlinear effects than those of Si. This influences the intense light energy fluxes and results in ULI conditions more difficult to be achieved in GaAs.

In this paper, we investigate the possibility to use high-repetition-rate trains of femtosecond pulses to address the challenge of ULI inside GaAs. This method is inspired by previous works revealing improved laser processing conditions by using high-repetition burst mode [10, 15–18]. A burst mode of irradiation allows replacing intense single pulses by trains of less intense pulses. In this way, plasma screening and other nonlinear propagation effects are reduced in the prefocal region to permit a higher deposited energy density at the focal position. However, to deliver enough energy density for material modifications, the repetition rate must be high enough to satisfy conditions leading to the accumulation of free carriers and heat on a pulse-by-pulse basis. Typically, the lifetime of the free carriers is on the order of few nanoseconds to hundreds of nanoseconds [19, 20]; and the heat dissipation time from a micrometer volume is typically a few nanoseconds [21–23]. Accordingly, repetition rates exceeding gigahertz are required to meet the demand of accumulation effect. In this paper, we use a tera-hertz (THz) repetition rate burst mode from which we expect accumulation effects to give their full potential and that can be implemented relatively easily in our experiments. For direct assessment of the benefits of THz burst mode irradiation inside GaAs, we rely on the luminescence microscopy technique [24] that was recently proposed for rapid 3D-monitoring of the achieved plasma densities and corresponding energy delivery inside GaAs. Several irradiation parameters, such as the number of pulses in the trains or temporal asymmetries in the pulse sequences, are optimized to perform the strongest achievable excitation densities. An important conclusion is a level of optimization that is superior to Si and which makes possible to cross the threshold for ULI inside GaAs using trains of femtosecond pulses. This opens up technological perspectives, an aspect that we illustrate with a stealth dicing demonstration.

2. Experimental setups

2.1. Laser sources and THz burst generation

In the experiments, we use a femtosecond laser source emitting pulses at a central wavelength of 1030 nm (Pharos, Light Conversion). Then, the wavelength is converted to 1550 nm by using an optical parameter amplifier (Orpheus, Light Conversion). While a GaAs crystal is in principle transparent to 1030 nm, the conversion to 1550 nm permits avoiding residual absorption by potential deep-level impurities typically introduced into GaAs crystal during its growth. This choice also facilitates the comparisons to previous studies performed in the domain of full transparency for Si. The pulse duration is around 180 fs as determined using a scanning autocorrelator. The source is operated at a repetition rate of 10 kHz and the pulse energy is controlled by a rotating half-wave plate and a polarizer.

To generate trains of pulses at THz repetition rate, we adopt a polarization splitting technique by passive propagation through engineered stacks of birefringent crystals [25, 26]. By propagation through a uniaxial birefringent crystal that is cut parallelly to the optical axis plane, linearly polarized incident pulses are decomposed along the fast axis and slow axis of the crystal, thus creating two temporally separated components (orthogonally polarized). The time delay between the components is then defined by the crystal thickness and birefringence. Accordingly, by stacking N crystals with increasing thicknesses according to $d_{n+1} = 2d_n$, a train of equally separated 2^n pulses can be generated. To exploit this method, we use yttrium orthovanadate (YVO_4) crystals (Altechna) with consecutive thicknesses of 0.25, 0.5, 1.0, 2.0, 4.0, and 8.0 mm. According to the birefringence of YVO_4 of $\Delta n = n_e - n_o = 0.214$ at 1550 nm, the splitting delays corresponding to the crystals are 0.18, 0.36, 0.71, 1.43, 2.85, and 5.71 ps, respectively.

In this work, we produce two types of pulse trains by using different configurations. As in previous studies, the first type consists of trains of pulses with equal intensity (square envelope). The optical configuration is shown in figure 1(a). The incident pulses have a linear polarization direction that is rotated 45° with respect to the fast axis of the first crystal. Accordingly, the following crystals always have a rotation of 45° with respect to the previous one. At last, a half-wave plate and a polarizer are placed. The half wave plate has either a rotation of 0° or 45° depending on the number of crystals (odd or even), while the direction of the polarizer is kept at 0° to always generate the same polarization for irradiation and ensure comparable measurements. The fixed polarization also avoids complications in the result interpretations potentially due to polarization-orientation dependent excitations. The shape of the produced pulse trains was verified by auto-correlation measurements in our previous publications concentrating on Si [10]. With such ultrafast trains of pulse,

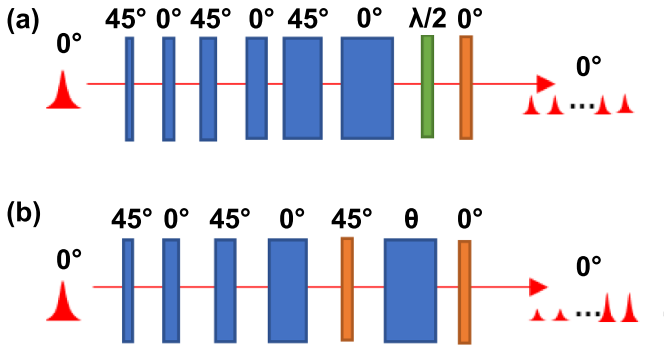

Figure 1. Birefringent crystal configuration for generating 'square' (a) or temporally asymmetric train of pulses (b). The birefringent crystals are represented with blue color with the angle of fast axis on the top, the half wave plate is represented in green, and the polarizer in orange with the transmission angle on top. The temporal shape of the pulse trains is represented in red with their polarization angle on top.

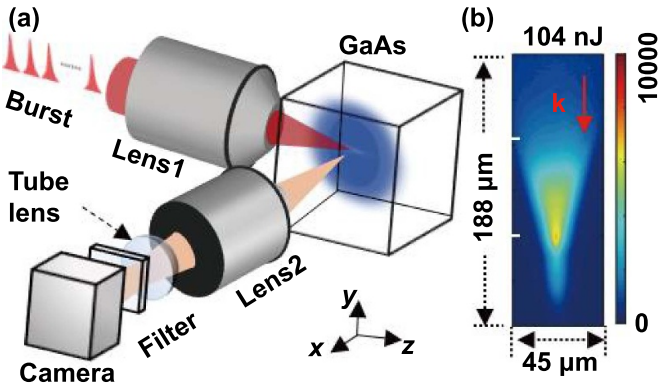

Figure 2. (a) Geometry of the setup for laser focusing inside the GaAs and luminescence microscopy diagnostic. (b) Example of the luminescence image obtained by single pulse excitation. The laser propagation direction is shown by the ***k*** vector. The employed energy for excitation and the scale of the image are written around the image. Note the 2:1 ratio between vertical and horizontal axis. These scales are the same for all the images in this manuscript unless specified. The colormap represents the pixel value (arbitrary units) in the map.

one can note that the irradiation conditions are approaching those of a longer pulse. However, it worth highlighting the square temporal profile in this asymptotic case. This strongly deviates to what we could obtain with a stretched Gaussian pulse. It is an important remark in regard of the strong dependence of this problem to the pulse shapes as revealed by recent works in Si [10]. Additionally, to enhance the delivered energy densities, we prepare a second strategy consisting in trains of pulses that are temporally asymmetric. The optical configuration used for this purpose is shown in figure 1(b). Similar to the previous approach, a train of 16 linearly polarized pulses is first produced using four crystals (with the thickness to be 0.5, 1, 2, and 4 mm, respectively) and one polarizer. Then the train propagates trough the thickest crystal (8.0 mm) resulting in 32 pulses that are split into two orthogonally polarized contributions of different intensity. Another polarizer with 0° angle is placed at the end to project the two orthogonally polarized components of the train after the final crystal on the same axis. This results in two-part ultrafast trains of pulses with a level of asymmetry (ratio of intensities between the two parts) simply varied by the rotation of the thickest crystal. The final shape of the obtained pulses and their auto-correlation measurements will be discussed in section 3.2.

2.2. *Laser irradiation and luminescence imaging*

For the laser irradiation experiments, the generated trains of pulses are focused 250 μm under the surface of the GaAs samples (Neyco, orientation (100)+/−0.3°, VGF growth method, intrinsic) by using a microscope objective (shown as Lens 1 in figure 2(a), 100×, NA 0.85, Olympus). The lens has a correction collar to compensate the spherical aberration induced by the refractive index mismatch at the interface between air and GaAs. An infrared microscopy system, consisting of another microscope objective (shown as Lens 2 in figure 2(a), 20×, NA 0.40, Mitutoyo), a tube lens, a short-pass filter (cutting wavelength at 1000 nm, DMSP1000R, Thorlabs), and an InGaAs camera (Raptor), is built to laterally image the focal region. Luminescence from the plasma can be observed due to the radiative band-to-band recombination of created free-carriers by nonlinear ionization [24]. The spectrum of the luminescence is peaking at 895 nm (1.38 eV). Accordingly, the short-pass filter (1000 nm) is simply used to suppress any parasitic light from the laser (1550 nm) during the measurement. While we use an InGaAs camera in this work for possible comparisons with pump-probe transmission imaging of the created plasmas (see [24]), it is worth noting it can also be replaced by a Si-based sensor for improved imaging performance of the luminescence signal. For images with adequate signal-to-noise ratio, the exposure time of the camera is set at 40 ms so each presented image corresponds to a luminescence signal accumulated over 400 pulses. A typical measured luminescence image is shown in figure 2(b). The results show the luminescence distribution emitted using a single pulse with an energy of 120 nJ (measured after the objective lens, Lens 1). Recently, we have shown that this luminescence can be a reliable method to directly map the 3D plasma densities [24] even under conditions that are hardly measurable by pump-probe shadowgraphy [23, 27]. This method will be used to analyze the achievable excitation densities in burst mode for GaAs and identify the most favorable irradiation conditions for internal processing.

A first interesting remark at this stage is an important dependence of the created luminescence to the setting of the correction collar for focusing. A maximum of emission is not necessarily corresponding to the optimal pre-compensation as expected from linear propagation. This indicates the possibility to partially pre-compensate some nonlinear propagation distortions by introducing spherical aberrations in the focused beams. However, to avoid accounting for these complex propagation aspects, all comparisons in this work are made with the correction collar systematically set at 300 μm. This deviates from the studied focusing depth (250 μm) but corresponds to conditions leading to the strongest luminescence

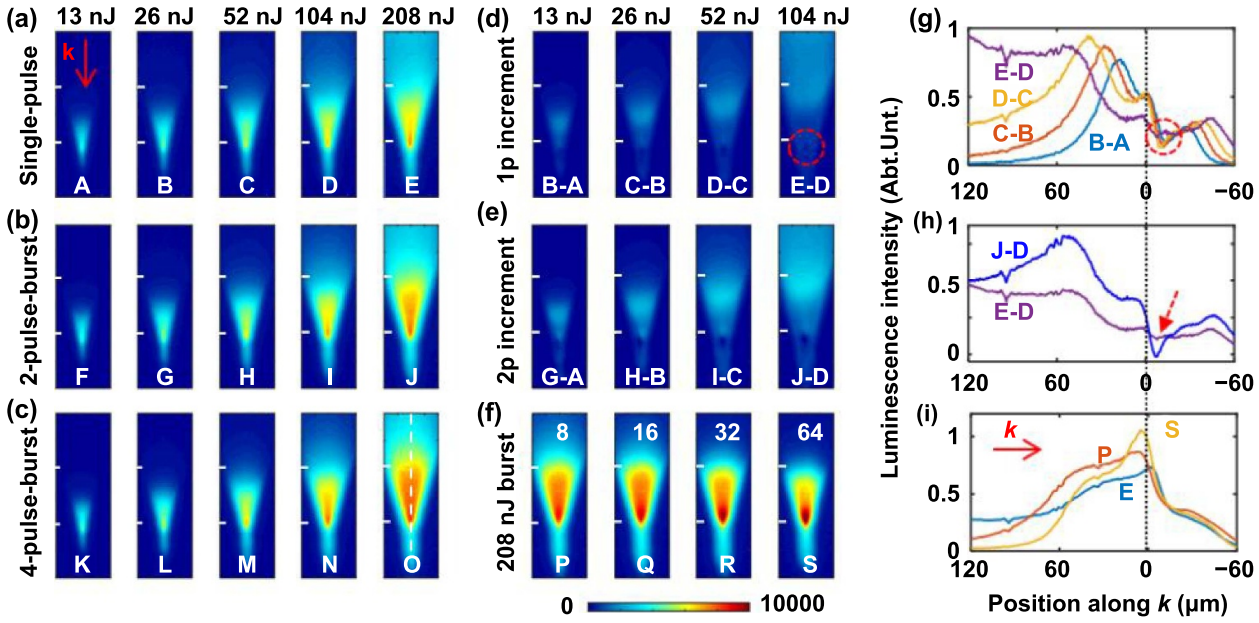

Figure 3. (a)–(c) The luminescence map excited by different pulse energies (written on the top) and different trains of pulses (written at the left). Each image is represented by a letter written at the bottom of the image. The ***k*** vector marks the laser propagation direction. (d), (e) subtraction of lower-energy maps on higher-energy maps according to the letters written at the bottom of the image. (f) Luminescence images all obtained from irradiations at 208 nJ energy in burst mode changing the number of pulses in the applied trains as indicated on the top of each image. (g)–(i) On-axis luminescence intensity signals (white dashed line in image *O*). The black dotted line represents the position of the geometrical focus ($z = 0$ μm).

signal for single pulses at the highest tested energy level (220 nJ). Under this condition, we try to optimize the number of pulses and temporal envelope of the applied trains to obtain the highest excitation densities.

3. Results and discussion

3.1. Comparative study of achievable excitation in burst mode

To compare the irradiation conditions and determine the optimal one, we first use luminescence microcopy to evaluate the characteristics of the plasmas generated by single-pulse irradiation at different pulse energies. The results are shown in figure 3(a). A strong asymmetry between the prefocal and postfocal regions can be immediately observed, indicating strong nonlinear propagation characteristics and plasma formation in the prefocal region. As the pulse energy increases, it appears that the plasma front moves backwards (opposite to beam direction), an aspect that has been identified as a severe limiting factor on the delivered peak intensity in semiconductors [9, 27–29]. Interestingly, these aspects can be directly monitored by the luminescence microscopy but not the pump-probe shadowgraphy due to the probe diffraction by a large and low-density plasma in the pre-focal region [14]. By simply subtracting one luminescence map from another obtained at lower energy, we can directly evaluate these aspects as well as the contribution of any extra applied energy. In figure 3(d), we show the result of the subtraction of luminescence from single pulses with consecutive increasing energies. For example, the first image of figure 3(d) shows the subtraction between the luminescence images obtained with pulses of 26 nJ (image *B*) and 13 nJ (image *A*). Similarly, the other images show the increment of plasma generation with higher energies. To provide a better insight, we plot in figure 3(g) the luminescence profiles along the optical axis (central profile at position marked by dashed line in image *O*). This representation confirms an increment of the luminescence signal and so excitation in the prefocal region. This is accompanied by a shift of the peak position prior to focus as the pulse energy increases. These results clearly highlight the difficulty to accumulate energy at the focal spot by simply increasing the pulse energy. In this regard, another interesting observation is the intensity void right after the focusing spot (marked by red dashed circle in figures 3(d) and (g)). This shows the development of a totally opaque over-dense plasma core, likely causing a final screening on the reduced energy approaching the geometrical focus. Overall, the measured plasma distributions show that attempts to deliver more intensity by increasing the pulse energy actually delocalize energy deposition rather than enhance it. Similarly to observations in Si [27, 30], there is then a severe saturation on the achievable local excitation that prevents the usability of single femtosecond pulses for internal structuring in GaAs. This is confirmed by the absence of permanent modification in all tested single-pulse cases in this study.

To evaluate the potential of the burst mode to solve this limitation by carrier accumulation, we thoroughly analyzed the case of trains of two pulses (delay = 0.18 ps) with the same total energy as for single pulses. The corresponding luminescence images are shown in figure 3(b). Interestingly, higher luminescence intensity is systematically observed in

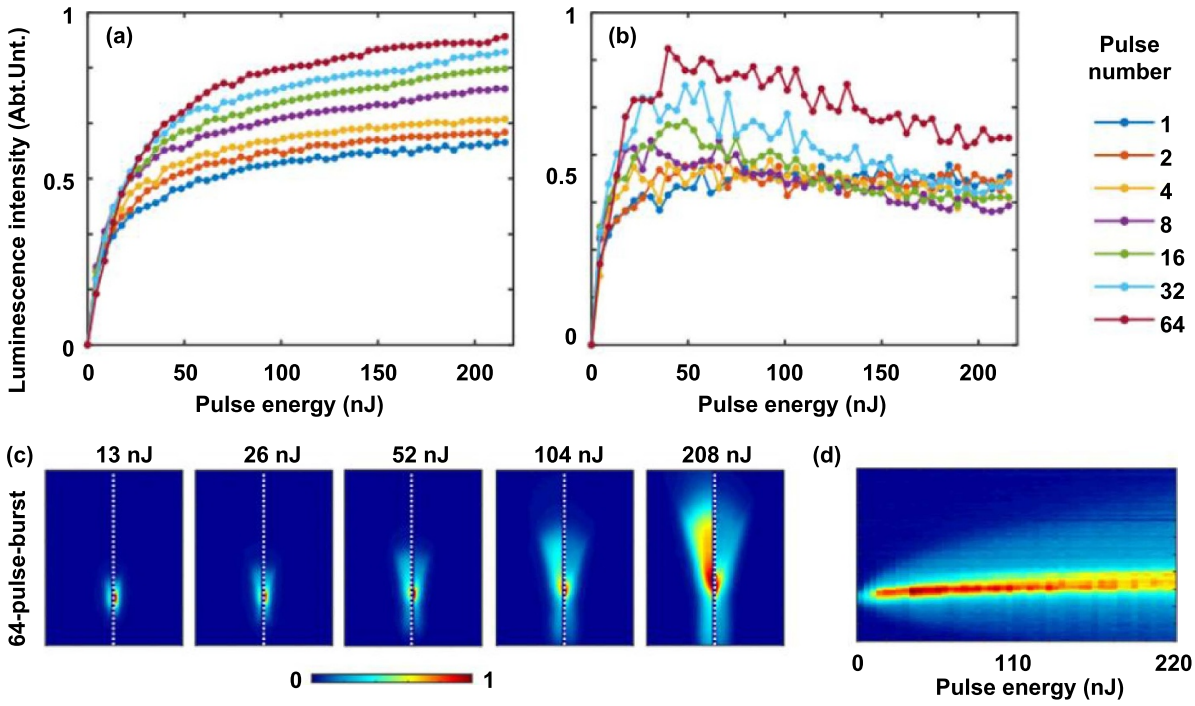

Figure 4. (a) Peak luminescence intensity from captured images as function of laser energy for different number of pulses in burst mode. (b) Corresponding peak luminescence signals from cross-section images obtained by Abel inversion. Figures (a), (b) share the same legend as shown on the right. (c) Captured images (on the left) and corresponding cross-sections as retrieved by Abel inversion (on the right) presented for 64-pulse trains at different energy levels (top labels). The size of each map is 188 μm (in vertical direction) and 38 μm (in horizontal direction). (d) Corresponding on-axis luminescence profile as function of the applied energy with 64-pulse trains.

comparison to single-pulse irradiation at the same total energy. To understand the benefit from splitting the energy in two-pulse trains on the achieved densities, we can subtract the single-pulse images at half intensity (figure 3(a)) from the double-pulse (figure 3(b)), thus obtaining the excitation map of the second pulse (figure 3(e)). For instance, the first image of figure 3(e) shows the subtraction of the single-pulse image *A* (13 nJ) from the image obtained with the train of two pulses at 26 nJ (image *G*). The result indicates an increment of plasma from the second pulse that can be compared to image *B–A* as the energy increase is the same. Similarly, the other images in figure 3(e) show the increment of luminescence from the second pulse at higher energy levels. An obvious difference with the single pulse case (figure 3(d)) is that the luminescence intensities near the focal spots are significantly higher for the double-pulse (figure 3(e)). This implies that the second approach allows a more efficient energy delivery at the focal plane and the possibility to rely on local energy accumulation up to a certain limit. To assess more clearly this point, we compare in figure 3(h) the on-axis luminescence from the images *E–D* and *J–D*. Remarkably, the comparison shows a higher signal prior to focus but also a more pronounced signal drop just after it (marked by red dashed arrow). This indicates the superior performance of the two-pulse train to deliver higher intensities but also the persistence of strong screening effects. The intensity maximum found about 50 μm prior to focus in image *J–D* reveals the region in which the first pulse creates screening conditions for the subsequent pulses. Obviously, this region enlarges with pulse energy, an aspect supported by the location of the maximum signal moving backward with increasing pulse energy in the images of figure 3(e).

To fully assess the degree of optimization in burst mode, we make similar luminescence measurements for trains of four pulses, as shown in figure 3(c). We can directly note a systematic increase of luminescence intensity compared to the previous cases. Likewise, if the number of pulses is further increased from 8 to 64, we observe that the peak signal keeps increasing at a fixed total energy. This is visible for the particular case of 208 nJ in figure 3(f); other energies can be found in supplementary material figure S1. These results unambiguously prove the effectiveness of the burst mode strategy as it allows carrier density accumulation at the focal spot and, in turn, higher absorbed energy densities. In figure 3(i), we quantitatively compare the on-axis luminescence profile for excitations at 208 nJ by using different number of pulses in the burst mode: 1, 8, and 64. It shows that as the pulse number increases, the luminescence intensity at the geometrical focus (near 0 μm, marked by black dashed line) increases while it decreases before the focal spot (further than 100 μm). This observation directly supports that the burst strategy effectively reduces the plasma generation in the prefocal region therefore benefiting the energy delivery to the focal spot.

To quantify the achievable local excitation, we select the peak luminescence value of each map and plot it in figure 4(a) as function of the applied energy with different number of pulses in the trains. For each burst case, the curves exhibit a similar trend, rapidly increasing at low energies and tending to

saturate on a plateau at high energy level. This shape is very similar to the previous measurements obtained by pump-probe shadowgraphy [27] applied to Si and showing the self-limited character of nonlinear ionization with focused femtosecond pulses. From figure 4(a), it must be noted that the burst mode of irradiation offers the possibility to significantly increase the maximum saturation level, with about a 50% increase from single pulse to the 64-pulse train.

Interestingly, we observe that despite the saturation trend, the maximum value still increases slowly, especially for trains with large number of applied pulses. At this stage, it is important to highlight a limitation of our imaging diagnostic method. The captured images rely from luminescence integrated in the depth of imaging field comparable to the plasma size. A consequence is an image that does not rigorously correspond to a cross-section of the plasmas. Therefore, the measurements do not directly reveal the core plasma conditions. To solve this issue, we can however take benefit from the cylindrical symmetry of the produced plasmas that makes possible a numerical retrieval of the emission cross-section by applying the inverse Abel transform algorithm. The detail of the algorithm is described in supplementary material note 1. The images before and after Abel inversion are shown in figure 4(c). For the ease of comparisons, the corresponding on-axis luminescence profiles are shown as function of applied energies in figure 4(d). This reveals a local maximum of luminescence at an energy level of about 50 nJ that does not confirm a monotonic increase of excitation with the applied energy seen with the integrated measurement. This is clear from presenting again in figure 4(b) the peak luminescence from the inverse Abel transforms as function of energy for the different tested pulse. Despite higher fluctuations due to the numerical retrieval procedure, in comparison to the integrated measurements in figure 4(a), we now observe a faster increase of the peak luminescence, followed by a slow decrease at increasing energies. This trend proves that the higher luminescence intensity at higher pulse energy in figure 4(b) can be attributed to the plasma size increment instead of a higher local excitation. The counter intuitive decrease of the local peak intensity for increasing incoming energy actually also corresponds well to previous experiments in Si [31, 32] revealing in some cases the existence of an energy window to make internal laser writing operational. Our local measurements confirm that excessive energy tends to deteriorate the local conditions and the potential for material modification in these situations.

3.2. Optimization with asymmetric trains of pulses

In the previous experiments, all the tested pulse trains have a square envelop (same energy for each sub-pulse). Moving forward, we investigate the possibility of further optimizing the energy delivery in burst mode by changing the train envelop. As a first step in this direction, we use the crystal arrangement described in figure 1(b) to generate a simple two-level asymmetric train of pulses. The theoretical temporal shapes of the generated trains are illustrated in figure 5(a). Each train comprises 32 pulses, but the intensity ratio between the first half (16 pulses) and the subsequent one can be continuously

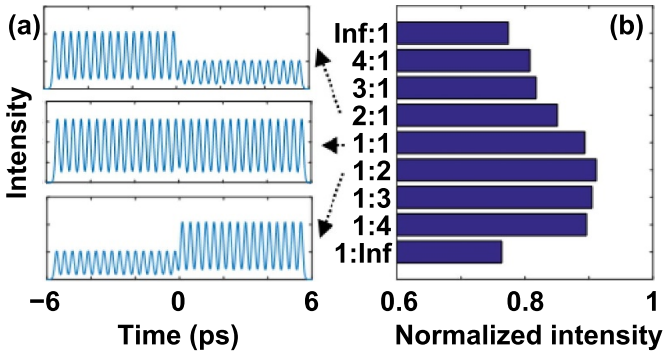

Figure 5. (a) Theoretical temporal profile of tested pulse trains of 32 pulses with intensity ratio of 2:1, 1:1 and 1:2 respectively. (b) The saturation excitation level obtained by trains with different intensity ratio. 'Inf' in the image represents infinite. Both 'Inf:1' and '1:Inf' are equivalent to the trains of 16 pulses.

adjusted. In figure 5(a), we exemplify the intensity ratios of 2:1, 1:1, and 1:2, respectively. Other ratios have similar temporal shapes as confirmed by auto-correlation measurements (results are shown in supplementary material figure S2).

Using the same luminescence measurement methodology, we performed a comparative study of achievable excitation densities with the asymmetric trains. For each tested asymmetry ratio, we captured luminescence images as function of the applied energy in a similar approach to section 3.1 (images are shown in supplementary material figure S3). We observe with this analysis a dependence of the saturation excitation to the asymmetry ratio. To make a quantitative comparison, we average the peak luminescence intensity obtained with energies from 120 nJ to 220 nJ, that is in the saturation regime according to figure 4(a). In this case we chose not to use the Abel inversion to represent the saturation results since the algorithm causes fluctuations making it difficult to reveal small differences. Interestingly, we observe that trains with a lower intensity in the front (i.e. intensity ratio of 1:2) are better performing than those of higher intensity in the front (i.e. intensity ratio of 2:1). This observation supports an optimum excitation with a progressively increasing energy delivery. Interestingly, an optimum intensity ratio of 1:2 is found among the tested conditions. Obviously, as we decrease this ratio, we tend towards a situation where the first half of the train barely contributes, and we return to the case of 16 pulses with square envelope. Exploring a ratio higher than 1:2 (see 'Inf:1' to '1:2' in figure 5(b)), the created plasma inevitably retro-acts on the trains creating it and causes a decrease of the excitation efficiency.

Limited by our experimental setups, we have investigated here very simple temporal shapes. The measured gain, despite modest (order of percents for 1:2 in comparison to 1:1), was clearly measurable as significantly above the measurement noise level (typically 0.5% as evaluated by statistical analyses). Further optimization can be expected if more complex trains are employed by means of more advanced temporal shaping techniques [33, 34]. Ultimate improvements in this context can be envisioned with individual control of the intensity of each applied pulses in the ultrafast trains. However, this

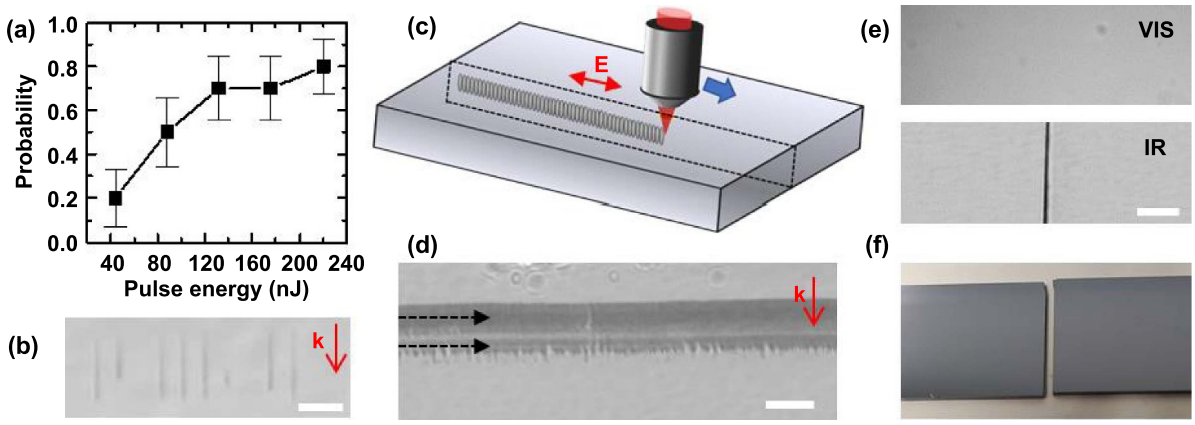

Figure 6. (a) Damage probability curve for GaAs irradiated with trains of 64 pulses. (b) Infrared images of ten irradiated regions at 220 nJ. The ***k*** vector marks the laser propagation direction. The scale bar is 20 μm. (c) Schematic representation of the laser writing configuration used for the GaAs stealth dicing demonstration. The polarization direction of the laser pulses is represented by ***E*** vector in the image. (d) Infrared lateral images of modified lines by dual scan (two depths) using burst mode irradiation. The dashed arrows mark the directions of the two scans. The scale bar is 100 μm. (e) Top view of the laser-written lines by visible-light microscopy for surface inspection (top image) and infrared-light microscopy revealing bulk modifications (bottom image). The scale bar is 100 μm. (f) Picture of separated GaAs chips along the laser-inscribed line after substrate bending.

will be associated to technological complexities and probably an over-dimensioned space of control parameters leading to the need of unrealistic resources for pure experimental pre-optimization studies. For future work, the use of appropriate simulation tools or artificial intelligence will be probably decisive in this regard.

3.3. *Fabrication and applications*

Even with the optimal conditions identified by the luminescence observations, it is worth highlighting at this stage that no permanent modification inside GaAs could be observed. However, it is possible to further optimize the focusing conditions to obtain even higher energy delivery like, for instance, changing the correction collar or shifting away from the theoretical plane that is free of spherical aberration. This is not surprising since the aberration correction of the employed focusing lens is only valid for linear propagation, which is not the current case.

Concentrating on the burst mode with 64 pulses with square envelop, we observed that if the focal plane is shifted around 100 μm closer to the surface, modifications appear as a consequence of deposited energy densities surpassing the material writing threshold. However, the threshold is not largely exceeded as trains of 32 or less pulses do not produce modifications applying the same final optimization procedure. This focus shift is another evidence of the presence of strong nonlinear propagation effects that are detrimental but, at the same time, can be partially compensated by introducing an appropriate level of spherical aberration in the focused beam [11]. The same way asymmetric pulse trains indicated possible optimizations in the time domain, a certain degree of optimization in the space domain could be addressed in future work using spatial light modulators or other flexible beam shaping technologies.

As a further step, we test the repeatability of the laser writing. Figure 6(a) shows the statistics of modification probability on the basis of ten repeated identical conditions at different pulse energies. For the writing attempts, each irradiation consists of 10 000 pulses obtained with 1 s exposure time with the laser operated at 10 kHz. It can be observed that the damage probability increases with the pulse train energy. However, the transition (energy window) from 0% to near 100% probability is very large indicating a rather stochastic process. Even with the highest tested pulse energy of 220 nJ, it is striking to note that the damage probability is not yet reliable (about 80%). Figure 6(b) shows the infrared microscopy images of the equal-condition modifications obtained using 220 nJ pulse trains. We observe non-repeatable modifications with different lengths. This stochasticity is due to the fact that the energy delivery conditions hardly exceed the threshold for writing. Therefore, the repeatability of modifications is prone to uncertainty from any fluctuation in the experimental conditions (i.e. surface or bulk material defects, energy instabilities). With trains of less pulses (32 or less), we confirmed that the probability for modification drops to zero for all tested cases.

Despite the instability of the writing process, this approach can be already used for manufacturing applications where repeated overlapping irradiations can be used to overcome the uncertainty problems as any previous modifications can serve as seeds to assist subsequent ones [5]. For example, in figure 6(c) we show the scheme of an experiment performed to create continuous lines inside GaAs. The configuration is similar to those used for stealth dicing experiments widely studied in Si [35]. In this approach, continuous under-surface modifications are required to avoid surface contamination and minimize the sacrificial zones. By applying our optimized femtosecond pulse bursts (64 pulses), we successfully fabricate continuous modifications inside bulk GaAs, as shown in figure 6(d). The lines are obtained by two inscriptions

at depths of 190 and 140 μm, respectively. In this way, a larger modified volume is obtained (in comparison to single-line writing at lower pulse energy for peak excitation conditions) in order to facilitate the targeted subsequent sample splitting process. The direction of the lines is aligned with one of the crystal axes along which it is possible to cleave the sample. The writing speed is 10 μm s^{-1}, corresponding to 1000 pulses per micron. Visible-light microscopy confirms no modification on the surface while top view infrared-light microscopy reveals the continuous internal structuring (figure 6(e)) obtained at these conditions. In figure 6(f), we illustrate a GaAs wafer that was easily split along the laser modification plane by simply bending the sample after laser processing. In view of this, the applications of the proposed method are not limited to stealth dicing but can be extended to many other applications where localized in-bulk modifications are required like embedded optical devices or in-wafer ingot marking.

4. Conclusion

In this paper, we investigate the possibility of using THz-repetition-rate burst mode for ULI inside GaAs, a material that cannot be internally processed with single femtosecond pulses. With the assistance of luminescence microscopy, we investigate the sensitivity of energy deposition to the characteristics of the applied pulses. The observations confirm a strong plasma in the prefocal region when using single pulses. This clearly screens the processing pulses resulting in a saturation and even a drop of the achievable fluence at the focal spot when the pulse energy is increased. By using the burst mode irradiation strategy, the plasma density in the prefocal region can be significantly reduced. This is beneficial for the energy delivery to the focal spots as revealed by enhanced luminescence signals. By preparing trains with increased number of pulses (up to 64), we observe a gradual enhancement of the energy delivery. Looking at the sensitivity to the characteristics of asymmetric trains and the level of aberration of the focused beam, we confirm further optimizations remain achievable in the temporal and spatial domains. With optimized square pulse trains, we successfully obtained bulk modifications inside GaAs. However, the modest repeatability of the burst mode writing process indicates that the delivered energy is just above the modification threshold. Despite this limitation we show that the writing process can be stabilized by continuous scanning of the sample as any seed modification allows (with appropriate irradiation overlap) creating modifications following the focus path anywhere in 3D inside GaAs. As a proof-of-concept, we show that the method can be directly applied for stealth dicing applications. More generally, this opens a wide variety of possible applications for fabricating undersurface structures inside GaAs, which holds strong potential for microelectronics and photonics applications.

Acknowledgments

This research has received funding from the European Research Council (ERC) under the European Union's Horizon 2020 research and innovation program (Grant Agreement No. 724480).

ORCID iDs

Andong Wang https://orcid.org/0000-0002-7760-0755
Pol Sopeña https://orcid.org/0000-0003-4112-3886
David Grojo https://orcid.org/0000-0002-8189-3781

References

[1] Sugioka K and Cheng Y 2014 Ultrafast lasers-reliable tools for advanced materials processing *Light Sci. Appl.* **3** e149
[2] Osellame R, Hoekstra H J W M, Cerullo G and Pollnau M 2011 Femtosecond laser microstructuring: an enabling tool for optofluidic lab-on-chips *Laser Photonics Rev.* **5** 442–63
[3] Tan D Z, Wang Z, Xu B B and Qiu J R 2021 Photonic circuits written by femtosecond laser in glass: improved fabrication and recent progress in photonic devices *Adv. Photon.* **3** 024002
[4] Al-Kattan A *et al* 2021 Short-pulse lasers: a versatile tool in creating novel nano-/micro-structures and compositional analysis for healthcare and wellbeing challenges *Nanomaterials* **11** 712
[5] Chambonneau M, Grojo D, Tokel O, Ilday F Ö, Tzortzakis S and Nolte S 2021 In-volume laser direct writing of silicon—challenges and opportunities *Laser Photonics Rev.* **15** 2100140
[6] Tokel O *et al* 2017 In-chip microstructures and photonic devices fabricated by nonlinear laser lithography deep inside silicon *Nat. Photon.* **11** 639–45
[7] Chanal M, Fedorov V Y, Chambonneau M, Clady R, Tzortzakis S and Grojo D 2017 Crossing the threshold of ultrafast laser writing in bulk silicon *Nat. Commun.* **8** 773
[8] Wang X Y, Yu X M, Berg M J, Chen P P, Lacroix B, Fathpour S and Lei S T 2021 Curved waveguides in silicon written by a shaped laser beam *Opt. Express* **29** 14201–7
[9] Wang A D, Das A and Grojo D 2020 Temporal-contrast imperfections as drivers for ultrafast laser modifications in bulk silicon *Phys. Rev. Res.* **2** 033023
[10] Wang A D, Das A and Grojo D 2020 Ultrafast laser writing deep inside silicon with THz-repetition-rate trains of pulses *Research* **2020** 8149764
[11] Chambonneau M *et al* 2021 Transverse ultrafast laser inscription in bulk silicon *Phys. Rev. Res.* **3** 043037
[12] Tokel O, Turnali A, Deminskyi P, Ilday S and Ilday F Ö 2018 Laser writing of nanostructures deep inside gallium arsenide (GaAs) *2018 Conf. on Lasers and Electro-Optics Pacific Rim (CLEO-PR)* (Hong Kong: IEEE) pp 1–2
[13] Bristow A D, Rotenberg N and van Driel H M 2007 Two-photon absorption and Kerr coefficients of silicon for 850–2200 nm *Appl. Phys. Lett.* **90** 191104
[14] Wherrett B S 1984 Scaling rules for multiphoton interband absorption in semiconductors *J. Opt. Soc. Am.* B **1** 67–72
[15] Sugioka K 2021 Will GHz burst mode create a new path to femtosecond laser processing? *Int. J. Extreme Manuf.* **3** 043001
[16] Caballero-Lucas F, Obata K and Sugioka K 2022 Enhanced ablation efficiency for silicon by femtosecond laser microprocessing with GHz bursts in MHz bursts(BiBurst) *Int. J. Extreme Manuf.* **4** 015103
[17] Kerse C *et al* 2016 Ablation-cooled material removal with ultrafast bursts of pulses *Nature* **537** 84–88
[18] Jiang L, Wang A-D, Li B, Cui T-H and Lu Y-F 2018 Electrons dynamics control by shaping femtosecond laser pulses in

micro/nanofabrication: modeling, method, measurement and application *Light Sci. Appl.* **7** 17134
[19] Callan J P, Kim A M T, Roeser C A D and Mazur E 2001 Ultrafast dynamics and phase changes in highly excited GaAs *Semicond. Semimet.* vol 67 (New York: Academic) pp 151–203
[20] Callan J P, Kim A M-T, Huang L and Mazur E 2000 Ultrafast electron and lattice dynamics in semiconductors at high excited carrier densities *Chem. Phys.* **251** 167–79
[21] Guo B, Sun J, Lu Y and Jiang L 2019 Ultrafast dynamics observation during femtosecond laser-material interaction *Int. J. Extreme Manuf.* **1** 032004
[22] Zhang D, Wu L-C, Ueki M, Ito Y and Sugioka K 2020 Femtosecond laser shockwave peening ablation in liquids for hierarchical micro/nanostructuring of brittle silicon and its biological application *Int. J. Extreme Manuf.* **2** 045001
[23] Mouskeftaras A, Chanal M, Chambonneau M, Clady R, Utéza O and Grojo D 2016 Direct measurement of ambipolar diffusion in bulk silicon by ultrafast infrared imaging of laser-induced microplasmas *Appl. Phys. Lett.* **108** 041107
[24] Wang A, Das A, Hermann J and Grojo D 2021 Three-dimensional luminescence microscopy for quantitative plasma characterization in bulk semiconductors *Appl. Phys. Lett.* **119** 041108
[25] Zhou S A, Ouzounov D, Li H, Bazarov I, Dunham B, Sinclair C and Wise F W 2007 Efficient temporal shaping of ultrashort pulses with birefringent crystals *Appl. Opt.* **46** 8488–92
[26] Dromey B, Zepf M, Landreman M, O'keeffe K, Robinson T and Hooker S M 2007 Generation of a train of ultrashort pulses from a compact birefringent crystal array *Appl. Opt.* **46** 5142–6
[27] Mouskeftaras A, Rode A V, Clady R, Sentis M, Utéza O and Grojo D 2014 Self-limited underdense microplasmas in bulk silicon induced by ultrashort laser pulses *Appl. Phys. Lett.* **105** 191103
[28] Kononenko V V, Zavedeev E V and Gololobov V M 2016 The effect of light-induced plasma on propagation of intense fs laser radiation in c-Si *Appl. Phys.* A **122** 293
[29] Mareev E I, Lvov K V, Rumiantsev B V, Migal E A, Novikov I D, Stremoukhov S Y and Potemkin F V 2020 Effect of pulse duration on the energy delivery under nonlinear propagation of tightly focused Cr:forsterite laser radiation in bulk silicon *Laser Phys. Lett.* **17** 015402
[30] Kononenko V V, Konov V V and Dianov E M 2012 Delocalization of femtosecond radiation in silicon *Opt. Lett.* **37** 3369–71
[31] Das A, Wang A D, Uteza O and Grojo D 2020 Pulse-duration dependence of laser-induced modifications inside silicon *Opt. Express* **28** 26623–35
[32] Chambonneau M, Lavoute L, Gaponov D, Fedorov V Y, Hideur A, Février S, Tzortzakis S, Utéza O and Grojo D 2019 Competing nonlinear delocalization of light for laser inscription inside silicon with a 2 μm picosecond laser *Phys. Rev. Appl.* **12** 024009
[33] Götte N, Winkler T, Meinl T, Kusserow T, Zielinski B, Sarpe C, Senftleben A, Hillmer H and Baumert T 2016 Temporal airy pulses for controlled high aspect ratio nanomachining of dielectrics *Optica* **3** 389–95
[34] Wang A D, Jiang L, Li X W, Wang Z, Du K and Lu Y F 2018 Simple and robust generation of ultrafast laser pulse trains using polarization-independent parallel-aligned thin films *Opt. Laser Technol.* **101** 298–303
[35] Kumagai M, Uchiyama N, Ohmura E, Sugiura R, Atsumi K and Fukumitsu K 2007 Advanced dicing technology for semiconductor wafer—stealth dicing *IEEE Trans. Semicond. Manuf.* **20** 259–65